BIOCHEMISTRY
including biophysical chemistry & molecular biology

Article

pubs.acs.org/biochemistry

Molecular Dynamics Characterization of Five Pathogenic Factor X Mutants Associated with Decreased Catalytic Activity

Safwat Abdel-Azeim,[†] Romina Oliva,[‡] Edrisse Chermak,[†] Raimondo De Cristofaro,[§] and Luigi Cavallo*[,†,∥]

[†]Kaust Catalysis Center, King Abdullah University of Science and Technology, Thuwal 23955-6900, Saudi Arabia
[‡]Department of Sciences and Technologies, University "Parthenope" of Naples, Centro Direzionale Isola C4, 80133 Naples, Italy
[§]Hemostasis Research Centre, Institute of Internal Medicine and Geriatrics, Catholic University School of Medicine, Rome, Italy
[∥]Dipartimento di Chimica e Biologia, University of Salerno, Via Papa Giovanni Paolo II, I-84084 Fisciano, Italy

Supporting Information

ABSTRACT: Factor X (FX) is one of the major players in the blood coagulation cascade. Upon activation to FXa, it converts prothrombin to thrombin, which in turn converts fibrinogen into fibrin (blood clots). FXa deficiency causes hemostasis defects, such as intracranial bleeding, hemathrosis, and gastrointestinal blood loss. Herein, we have analyzed a pool of pathogenic mutations, located in the FXa catalytic domain and directly associated with defects in enzyme catalytic activity. Using chymotrypsinogen numbering, they correspond to D102N, T135M, V160A, G184S, and G197D. Molecular dynamics simulations were performed for 1.68 μs on the wild-type and mutated forms of FXa. Overall, our analysis shows that four of the five mutants considered, D102N, T135M, V160A, and G184S, have rigidities higher than those of the wild type, in terms of both overall protein motion and, specifically, subpocket S4 flexibility, while S1 is rather insensitive to the mutation. This acquired rigidity can clearly impact the substrate recognition of the mutants.

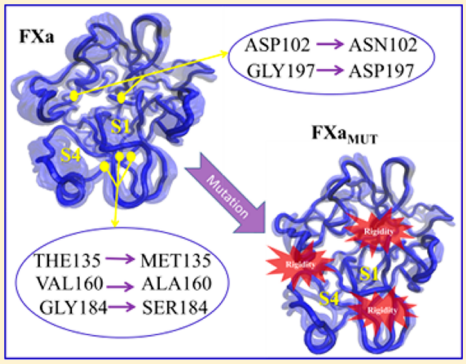

Factor X (FX) is a plasma vitamin K-dependent serine protease,[1,2] and one of the major players in the coagulation cascade. It is the point of convergence between two pathways, which lead to the formation of blood clots (fibrin), i.e., the contact activation pathway (or intrinsic pathway), and the tissue factor pathway (or extrinsic pathway).[3] FX is activated to FXa through the cleavage of the Arg194−Ile195 peptide bond (Arg15−Ile16 peptide bond in chymotrypsinogen numbering) by the factor IXa−factor VIIIa−phospholipid−calcium complex in the intrinsic pathway, and by the factor VIIa−tissue factor−phospholipid−calcium complex in the extrinsic pathway. After activation, FXa interacts with factor Va to form the prothrombinase complex, which activates prothrombin to thrombin. In the final stage of the blood coagulation cascade, thrombin, in turn, converts fibrinogen into fibrin.[4,5]

The tertiary structure of the FXa catalytic domain is composed by two six-strand β-barrels and four short helices (see Figure 1).[6−8] The N-terminal barrel consists of strands β2−β7, whereas the C-terminal barrel consists of strands β8−β13, with the participation of a two-residue strand (β1) from the N-terminal tail. Four helical segments are also found between β4 and β5, β7 and β8, and β9 and β10 and after the last β13 strand, which are named H1−H4, respectively. The three serine protease catalytic residues His57, Asp102, and Ser195 (chymotrypsinogen numbering) are located at the crevice between the two barrels.[9] The FXa−substrate/ligand interaction is mainly controlled by four binding site subpockets (S1−S4). Subpocket S1, with an anionic character given by

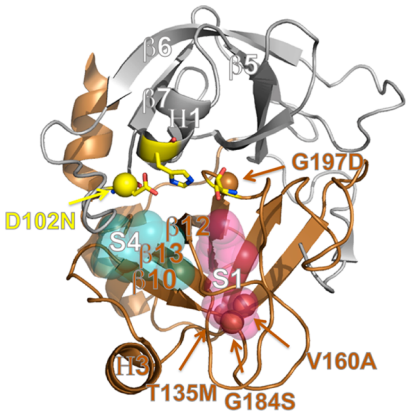

Figure 1. Cartoon representation of the crystallographic structure of the catalytic domain of human FXa (Protein Data Bank entry 2BOH). In this orientation, the N-terminal β-barrel is up (gray) and the C-terminal β-barrel is down (copper). Residues of the catalytic triad are shown as yellow sticks. The Cα atoms of residues corresponding to the five selected mutations are shown as spheres. The S1 and S4 subpockets are colored pink and teal, respectively. Secondary structure elements discussed in the Results are labeled.

Received: June 22, 2014
Revised: September 19, 2014
Published: October 14, 2014

 © 2014 American Chemical Society dx.doi.org/10.1021/bi500770p | *Biochemistry* 2014, 53, 6992−7001

residue Asp189, is also lined by residues Gln192 and Tyr228, and by the backbone of residues 190, 191, 214−216, and 225−227,[9] and represents the major player in selectivity and binding.[10] The main interaction of S1 is a salt bridge between Asp189, at the bottom of the subpocket, and an Arg residue or a positively charged fragment from the substrate/inhibitor. Subpocket S2 is small, shallow, and not well-defined. It merges with subpocket S4, which is aromatic in nature, being lined by residues Tyr99, Phe174, and Trp215. Subpocket S4 is mainly involved in hydrophobic interactions between FXa and its natural substrates, although it has recently been observed to be involved in the binding of organic ligands designed to establish cation−π interaction.[11,12] Finally, subpocket S3 is located on the rim of the S1 pocket and is quite exposed to the solvent.[10]

On a physiological level, FX deficiency causes hemostasis defects, like intracranial bleeding, hemathrosis, and gastrointestinal blood loss.[13] On the other hand, FXa is one of the main targets among activated coagulation factors for new oral antithrombotic drugs, globally defined as Xabans. These drugs, which are direct inhibitors of the active site of FXa, are already being used in therapy for the prevention of stroke in atrial fibrillation and the treatment of acute and chronic venous thromboembolism.[14−16] Inherited FX deficiency is a rare coagulopathy with severe bleeding symptoms presenting early in life in homozygous patients.[3,17] As effective therapies are needed to control excessive bleeding for a range of clinical conditions,[18,19] a detailed understanding of the FX catalytic activity would be of great interest. To date, more than 100 naturally occurring mutations have been identified in the FX gene, from which important insight into the FXa structure and function could come. However, only few FX mutants have been expressed and characterized; only 10 of them have presented substitutions located in the catalytic domain.[3,20,21] Moreover, not all the catalytic domain mutants characterized to date have been found to directly affect FX catalytic function. For instance, the Arg347His/Asn mutants act by perturbing the interface between FXa and its cofactor FVa.[22]

In this work, we have undertaken a molecular dynamics (MD) study of a pool of mutants selected to be located in the FXa catalytic domain and to be directly associated with defects in enzyme catalytic activity. In particular, selected mutants satisfy the following criteria. They all (i) have been identified in patients suffering from bleeding symptoms, (ii) show a normal or near-normal FX antigen level in culture media (thus suggesting that the mutants do not impair FX biosynthesis or secretion) and normal activation, and (iii) exhibit a dramatic decrease in catalytic activity toward the FXa natural substrate (prothrombin), compared to the wild-type enzyme.[23−28] The five FX mutants, selected on the basis of the criteria mentioned above, are listed here in chymotrypsinogen numbering, which will be used throughout the text, while the original numbering is given in parentheses: D102N (D282N[26]), T135M (T318M[27,28]), V160A (V342A[23]), G184S (G366S[24]), and G197D (G381D[25]). All five mutated residues are widely conserved within FX members, with only Thr135 undergoing a conservative mutation to Ser in few species, such as horse. They exhibit instead different conservation rates among the whole set of human serine proteases involved in the blood coagulation cascade (see the sequence alignment in Figure S1 of the Supporting Information). In particular, while Asp102, Gly184, and Gly197 are fully conserved and Val160 undergoes only conservative mutations (to Leu and Ile), Thr135 is substituted with a variety of different amino acids (however, not including Met). Interestingly, the mutants mentioned above are spatially well concentrated in two specific enzyme regions (see Figure 1). In particular, D102N and G197D are located in or close to the catalytic triad, Asp102 being part of the triad and Gly197 being only two residues downstream from the catalytic Ser195. The three remaining mutants, T135M, V160A, and G184S, although located at the N- or C-terminus of different strands, occupy a well-defined region just behind the negatively charged Asp189, at the bottom of the S1 subpocket. This structural order has been adopted in the following figures and tables. Our MD simulations allowed us to gain detailed insight into the factors controlling FXa activity, especially with regard to the substrate recognition process.

METHODS

MD simulations of the wild type (WT) and the selected mutants, D102N, T135M, V160A, Gl84S, and G197D, of the FXa enzyme in the unbound ligand state were performed with GROMACS version 4.6.[29] The MD simulations were initialized from the high-resolution X-ray structure of Nazare et al. (Protein Data Bank entry 2BOH, 2.2 Å resolution).[10] The flexible light chain was removed, while the heavy chain and the calcium ion were kept. We also kept all 174 crystallographic waters, because a previous MD study indicated that inclusion of crystallographic waters in the starting structure leads to more stable and better performing MD trajectories.[30] The starting structure for the FXa mutants was generated by Modeller version 9.10 using 2BOH as a template.[31] MD simulations of WT FXa and the mutants were performed using the AMBER99SB[32] force field and the TIP3P model for the water molecules.[33] The structure of the WT and those of the mutants were solvated in a periodic cubic water box with a buffer distance of 10 Å between the protein and the box edges. To obtain an electrically neutral system, the GENION tool from the GROMACS package was used to randomly replace water molecules with the appropriate number of counterions. The total number of water molecules and the total number of chloride ions added to the systems are 12660 and 3 for WT, 11285 and 4 for D102N, 11629 and 3 for T135M, 11929 and 3 for V160A, 11878 and 3 for G184S, and 11209 and 2 for G197D, respectively. The systems were energy minimized with the steepest descent method to a convergence on the maximal force of 100 kJ mol^{-1} nm^{-1}, followed by a short 100 ps *NVT* at 300 K and 100 ps *NPT* MD simulation at 300 K and 1 atm to equilibrate the systems. During equilibration, harmonic constraints were applied on the heavy atoms of the protein. Four different *NPT* MD simulations for both the FXa and mutant structures were conducted at 300 K and 1 atm for 60 ns assigning different initial velocities. The particle mesh Ewald (PME) algorithm[34] was applied to treat long-range electrostatic interactions. The protein and the solvent were independently coupled to a thermal bath by a Berendsen thermostat[35] with a time constant of 0.1 ps. Pressure was controlled with a Parrinello−Rahman barostat[36] with a time constant of 2 ps. The time step of the simulations was set to 2 fs, and the coordinates were saved at regular intervals of 10 ps. Structural properties such as the root-mean-square deviation (rmsd) and the root-mean-square fluctuation (rmsf) were calculated with GROMACS standard analysis tools. Hydrogen bonds were calculated using cutoffs on the donor−acceptor heavy atom distance and the hydrogen−donor−acceptor angle of 3.5 Å and 30°, respectively, using HBonanza.[37] The principal component analysis (PCA)[38−41] calculations were performed on a

dx.doi.org/10.1021/bi500770p | *Biochemistry* 2014, 53, 6992−7001

combined trajectory composed of the last 50 ns of each of the four simulations. The frames of the combined trajectory were superimposed on the first frame to remove overall rotations and translations of the systems. The PCA was performed by diagonalization of the covariance matrix of the Cα fluctuations using standard GROMACS tools. PCA figures and movies were generated using the NMWIZ plugin[42] in Visual Molecular Dynamics (VMD).[43] The volumes of subpockets S1 and S4, which control the interaction of FXa with the substrate, were monitored with MDpocket.[44] To select the spheres defining the two subpockets, Mdpocket was initially run on the first trajectory for each system. All the frames analyzed were superimposed on the initial structure, and the spheres defining the pockets were generated with MDpocket default parameters. The spheres clustered around subpockets S1 and S4 (see Figure S2 of the Supporting Information) were used to calculate the volume of the subpockets in all the trajectories. Isolated spheres, even if they are assigned to the S1 and S4 subpockets by MDpocket, were eliminated. To achieve smoothed volume profiles, volumes were averaged over the four trajectories using a 100 ps window.[44,45]

Analysis of the contacts between the two barrels of FXa in the X-ray structure and the evolution of the interbarrel contact during the dynamics was performed with COCOMAPS and MDcons.[46,47] Within the COCOMAPS and MDcons analyses, two residues are considered to be in contact if at least two heavy atoms are separated by ≤5 Å. This is the definition used in the CAPRI (Critical Assessment of Predicted Interactions) experiment, and we used it for the sake of consistency with a well-established and largely accepted protocol.[48−50]

RESULTS

Monitoring MD Trajectories. The analysis of the sampling convergence was performed by computing the root-mean-square inner product (rmsip) of the first 10 eigenvectors from PCA of the four replicas for each system. rmsip measures the similarity between subspaces defined by the basis vectors obtained from the PCA calculations. The estimated rmsip values (see Table S1 of the Supporting Information) confirm the high degree of similarity between the space sampled by the four replicas, with minimum rmsip values around 0.65 (values of 0 and 1 indicate no overlap and perfect overlap, respectively).

Both the WT and all five considered FXa mutants are stable during the whole dynamics, with maximal rmsd values on the Cα atoms not exceeding 2 Å from the initial structure. Most of the systems display an average rmsd value of 1.3 Å in the last 10 ns of the MD simulations (see Figure 2), with V160A being slightly more rigid. Overall, the rmsd values are indicative of limited conformational changes.

Analysis of the Cα atom rmsf results in rather similar profiles (see Figure S3 of the Supporting Information). WT, T135M, and V160A have a maximal rmsf value of roughly 2.5 Å, while G197D, D102N, and G184S have a maximal rmsf value of 1.8 Å, thus appearing to be even less flexible than the WT and the other mutants. Therefore, none of the examined mutations seems to perturb the overall folding of FXa.

Principal Component Analysis (PCA). PCA is a valuable technique for identifying the slow modes that can be related to protein function.[51−53] We have analyzed the MD trajectories of WT and the five mutants using the PCA technique to get an idea about the essential motions that may be related to the different experimental catalytic efficiencies. The free energy surface of a protein can be obtained using a conformational sampling method that allows exploration of the conformations near the native state structure. This type of analysis is routinely used in the MD community to get an idea about the equilibrium sampled states.[54−59] PCA was conducted on the Cα atoms, considering a combined trajectory of the four simulations for each system, in the 10−60 ns window. Comparison of the dominant motions between the WT FXa and its mutants allows the characterization of the structural changes induced by each mutation. The rmsip values for the first 10 eigenvectors from PCA of the mutants and of the WT are in the range of 0.64−0.68, which indicates a reasonably good level of similarity between the overall motion in the mutants with respect to the WT (see Table S2 and Figure S4 of the Supporting Information).[60] Further, the first five PC modes contribute to 40−50% of the overall motion of the systems, with the first two modes contributing 25−35% (see Figure S5 of the Supporting Information). Although the contribution of the first two modes is not particularly large, it is in line with the contribution found in similar analyses.[61,62] Moreover, the free energy surface of the projection of the whole combined trajectory in the space of the third and fourth modes shows a minimum centered at the origin (see Figure S6 of the Supporting Information), which indicates fluctuations around the starting conformation, thus providing scarce information about possible large scale conformational changes. The greater relevance of the first two modes is also supported by the clearly larger first two eigenvalues from the PCA, together with the clearly larger amplitudes of the Cα atom fluctuations for the first two modes compared to modes 3−5 (see Figure S5 of the Supporting Information). Therefore, further analysis of the protein motion will be done only considering the first two modes, as they capture the largest part of the essential motions of the protein.

If a focus is thus placed on the first two modes, inspection of the displacement of the Cα atoms along the modes (Figure 3), which is commonly used to identify the residues contributing to a specific mode,[62−64] indicates that the mutants behave like the WT except for few positions, where some mutants present different peaks. In particular, mutant T135M has fluctuations that are larger than those of the WT and the other mutants around residues 145−150, as a consequence of large fluctuations in two of the four simulations (see Figure S7 of

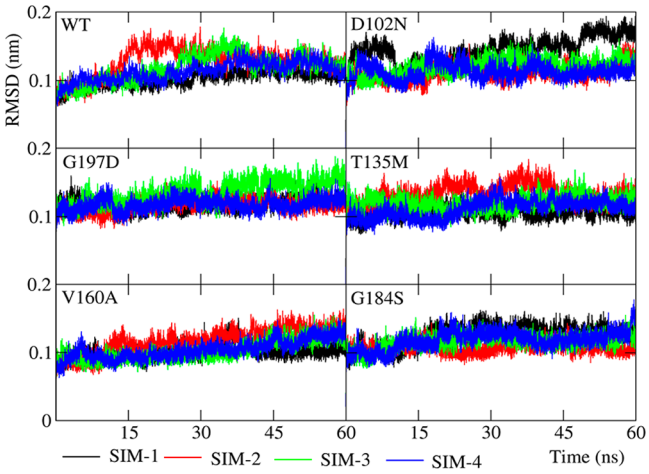

Figure 2. rmsd from the starting structure, calculated on the Cα atoms, for the four trajectories of the WT and the mutants.

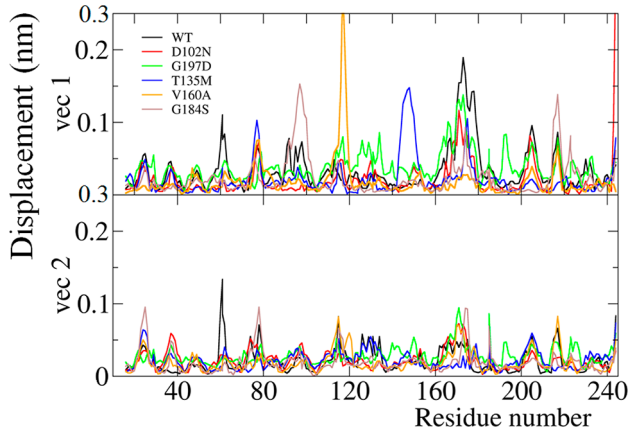

Figure 3. Displacement of the Cα atoms along the first two PCA modes (PC1 and PC2) for WT FXa and the considered mutants.

the Supporting Information), while V160A has larger fluctuations in the segment of residues 116−119, because of a remarkably large fluctuation in one of the four simulations (see Figure S7 of the Supporting Information). However, it is worth remarking that the occurrence of a large fluctuation in a single trajectory cannot be considered statistically significant.

PC1 of the WT involves the substrate binding subpockets, with flexibility around residues 94−97, resulting in flexibility at the border of subpockets S1 and S4, as well as of the loops connecting the secondary structure elements H1 and β5 (amino acids 61−64), β6 and β7 (amino acids 91−103), and H3 and β10 (amino acids 173−179), and the N-terminal part of the loop connecting β12 to β13 (amino acids 216−219). Overall, this mode corresponds to a breathing movement of the protein, which controls the opening of subpockets S1 and S4, as evidenced in the visual representation of this mode, shown in Figure 4.

Three of the loops mentioned above indeed include residues defining the S1 and/or S4 subpocket. Detailed analysis of the dynamics of subpockets S1 and S4 is discussed in a following section, while animations of PC1 are shown in the Supporting Information. Further important fluctuations correspond to α-helix H3 (residues 164−172), which is involved in the interaction with coagulation factor Va.[65] Interestingly, the flexibility of the mutants in the region involving the border of subpocket S1 is lower than that of the WT, with T135M, D102N, and especially V160A showing particularly high rigidities in this area. Mutant G197D shows a flexibility similar to that of the WT at the border of subpockets S1 (around residues 191−195) and S4, although this motion impacts only S1 and is opposite in direction to that of the WT, thus keeping the subpocket S4 open (compare the two modes shown in Figure 4). Mutants G184S and V160A share the same movement at the S1 border (loop connecting β12 and β13), which again is opposite in direction to that of the WT. However, V160A shows high rigidity over all the structure, while the movement of G184S is closer in amplitude to that of the WT. Furthermore, G184S has another movement at the bottom of S1 (residues 220−224) opposite to the movement at the top of S1 (residues 216−219). Therefore, in it the opening of subpocket S1 is very limited. Interestingly, V160A is highly rigid, despite the mutation being relatively far from the catalytic triad and from subpockets S1 and S4. Finally, T135M is the only system presenting a quite larger peak in the region of residues 140−160, which may be related to the loss of specific

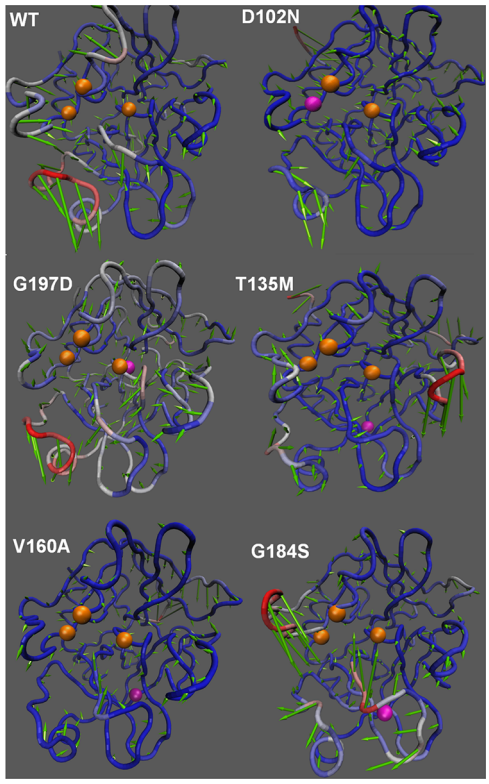

Figure 4. Porcupine representation of the first PC mode of WT FXa and its mutants. The orange spheres indicate the positions of the catalytic triad, and the magenta spheres indicate the positions of the mutations. Green arrows indicate the direction of motion along PC1. Flexibility ranges from high (red) to low (blue).

H-bonds due to the mutation, in particular between residues Thr/Met135 and Glu159 (see below).

The PC2 profile is quite similar to the PC1 profile, the difference being that the highly flexible part is moved from helix H3 to helix H1 (residues 55−61). Nevertheless, no highly flexible region emerges from the profile of Figure 3. A visual representation of this mode, for all the systems, is shown in Figure S8 of the Supporting Information. Inspection of Figure S8 of the Supporting Information indicates comparable or even higher flexibility of the mutants, as in the case of G197D, than of the WT. However, the increased flexibility of G197D does not correspond to an increased level of opening of subpocket S1. V160A, which was much more rigid than the WT, according to PC1, exhibits a collective motion around subpocket S1 very similar to that of the WT; nevertheless, as indicated by the fluctuations shown in Figure 3, this movement is very limited compared to that of PC1. PC2 of G184S shows instead a rigidity even higher than that of PC1, especially at S1 and the catalytic triad site.

As for the overall movement of the protein, the free energy surface from the projection of the whole trajectory in the space of the first two essential modes (Figure 5) results in multiple minima for several of the systems, indicative of different and well-defined conformational states sampled by several of the systems. For example, the free energy surface of the WT shows two broad minima at PC1 values of roughly −1 and +1, with an additional narrower minimum at PC1 values close to +1, and the possibility that the two minima at PC1 close to +1 could converge into a single broad minimum with longer simulation times cannot be excluded. Similarly, it has to be kept in mind

dx.doi.org/10.1021/bi500770p | Biochemistry 2014, 53, 6992−7001

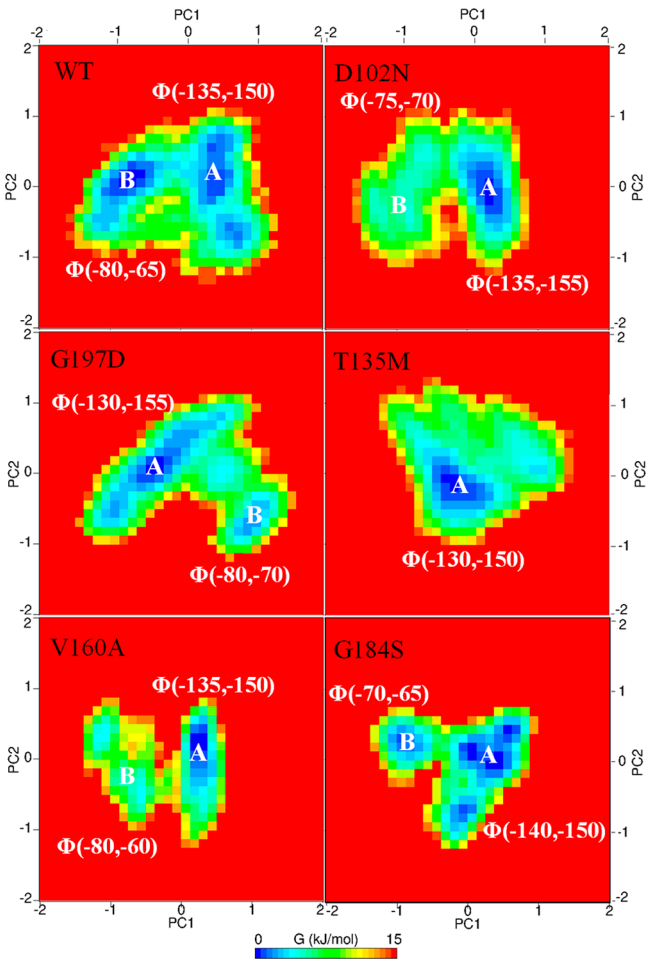

Figure 5. Free energy surface of WT FXa and its mutants in the space of the first two PCA modes (PC1 and PC2). Displacement along PC1 and PC2 is in nanometers. The contour map resolution is 1 kJ/mol. The dihedral Φ angles are reported in parentheses for Phe174 and Trp215, respectively.

that the depth of the various minima of all the systems could still change with longer simulation times. To gain an understanding of the convergence of the free energy surface, we plotted the WT free energy surface at different sampling times (see Figure S9 of the Supporting Information). Comparison of the surfaces of Figure S7 of the Supporting Information indicates that the free energy surface is quite converged after 160 ns. This supports the presence of distinct and well-defined conformational states, whose characterization is performed in the next section.

Finally, the traces of the covariance matrix, which account for the overall amount of motion, decrease in the following order: WT (1.81) ≈ G197D (1.78) > D102N (1.60) > T135M (1.56) > V160A (1.51) > G184S (1.46). This indicates that G197D has a flexibility comparable to that of the WT, while all the other mutants have clearly lower flexibility.

Analysis of the FES Minima. To correlate the FES minima and the conformational changes occurring during the MD simulations, we have extracted and analyzed several structures with PC1 and PC2 values at the center of each minimum. The representative structures of the two minima of the WT FES (A and B) show differences at the level of the S4 subpocket, specifically at residues Phe174 and Trp215 (see Figure S10 of the Supporting Information). Analysis of structures corresponding to the two minima in the FES of all the mutants (with the exception of T135M, whose FES has only one minimum) also highlighted the fact that the two minima are essentially characterized by different behavior around residues Phe174 and Trp125. Because the side chains of Phe174 and Trp215, together with Tyr99, shape the aromatic S4 subpocket, we focused on a detailed analysis of the distribution of dihedral angles of these three residues. While the distribution of the ϕ and ψ angles of Tyr99 is well centered around a single value, the distribution of the ϕ angle in Trp215 and Phe174 clearly shows two peaks (see Figure 6). For Phe174, the two peaks are

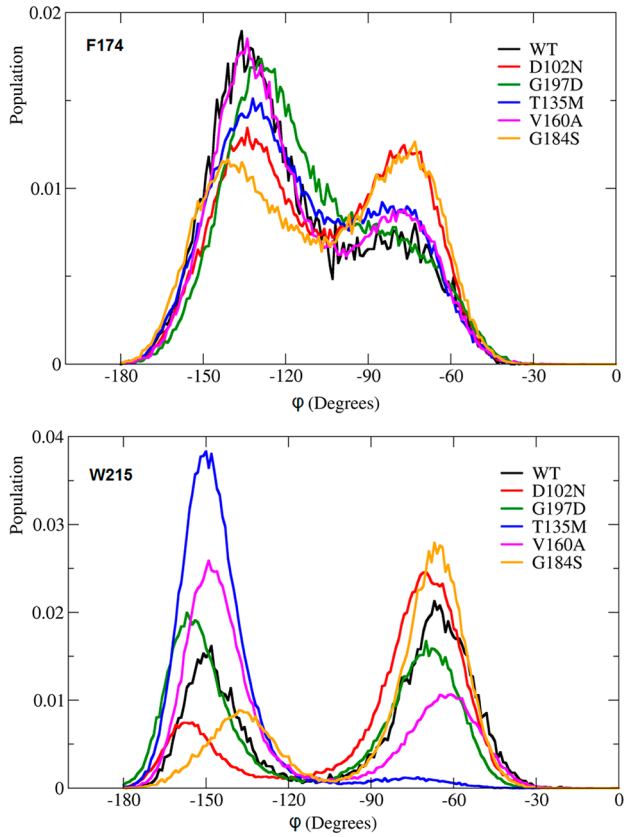

Figure 6. Dihedral populations of the backbone dihedrals φ of Phe174 and Trp215, extracted from the combined trajectory of 200 ns.

centered at ϕ values of approximately −130° and −75° and largely overlap, with the former corresponding to the value in the X-ray structure of 2BOH. In Trp215, instead, the two peaks are well separated and centered at ϕ values of approximately −65° and −150°, the value of the X-ray structure. Interestingly, while the shape of the ϕ distribution for Phe174 is similar in all the systems, although the peak at a ϕ value of approximately −75° is only a shoulder for the WT and a well-defined peak for G184S and D102N, the ϕ distribution for Trp215 shows significant differences between the various systems. Indeed, for the WT and G197D, the two peaks have almost the same height, while the other systems clearly prefer one of the conformations. Specifically, D102N and G184S prefer the $\phi \approx -65°$ conformation, whereas V160A and T135M prefer the $\phi \approx -150°$ conformation. Actually, in the case of T135M, only the $\phi \approx -150°$ conformation is sampled, which is consistent with the single minimum in the FES of Figure 5. The structure corresponding to the various minima for all the systems is shown in Figure S10 of the Supporting Information.

dx.doi.org/10.1021/bi500770p | Biochemistry 2014, 53, 6992−7001

As a conclusion for this section, it is clear that conformational changes around subpocket S4 diversify the various systems. The consequences of these changes, in terms of subpocket features, will be discussed below.

Hydrogen Bond Analysis. The average number of H-bonds from the combined simulations of the WT and mutated FXa systems is reported in Table 1. Three mutants, G197D, V160A, and G184S, have on average 1.7−3.9 more H-bonds than the WT, whereas T135M and D102N have approximately one fewer H-bond than the WT. In the following, we provide a short analysis of the main H-bonds affected by the mutations, taking the WT as reference for these changes (for more details, see Table S3 and the text of the Supporting Information).

Table 1. Average Numbers of H-Bonds, and the Relative Standard Deviations, from a Cumulative Analysis of the Four MD Trajectories for Each System

	average	standard deviation
WT	170.3	6.4
D102N	169.2	6.6
G197D	172.0	6.6
T135M	169.6	7.3
V160A	173.7	6.6
G184S	174.2	6.2

H-Bonds most impacted in the mutants are located in the C-terminal barrel, which is reasonable considering that, with the exception of D102N, all the mutations are located in this barrel. For instance, in G197D and G184S, a H-bond not observed in the WT is formed between Asp126 (bb) and Ser130 (sc). With regard to changes directly linked to the mutation site, the H-bond between the side chains of the catalytic Asp102 and His57, 90% populated in the WT, is completely lost in the D102N mutant. Analogously, the H-bond between Thr135 (sc) and Glu159 (sc), 68% populated in the WT, is lost in T135M. Another example is in G184S, where, on the contrary, two additional H-bonds are formed by the side chain of the Ser in the mutant, with Gly226 (bb) and Asp189 (sc). A similar perturbation of the H-bonds also affects the interface between the two barrels, i.e., the substrate crevice. For example, the WT H-bond between Gly40 and Gln151 (sc) is completely lost in G197D and G184S.

Interestingly, in many instances, the same H-bond is perturbed in more than one mutant, confirming that the effect of the point mutations extends to long distances and suggesting that the H-bonds mainly affected by mutation may represent points of weakness in FXa global folding.

Analysis of the Interface between the Two Barrels. To understand if the mutations alter the interaction between the protein N- and C-terminal barrels, we analyzed the dynamic behavior of the interface between the two barrels using COCOMAPS and MDcons, two tools we developed for analyzing the static and dynamic features of the interface in protein−protein complexes.[46,47]

The interbarrel residue−residue contact map of the X-ray structure of the WT, shown in Figure 7a, indicates that the interaction between the two barrels is essentially hydrophobic in nature, with the exception of one clear hydrophilic patch between amino acids 70 and 75 on the N-terminus and amino acids 150 and 155 on the C-terminal barrel.

The total number of interbarrel contacts in the X-ray structure amounts to 192, corresponding to an interface area of 2281 Å^2. MDcons overall conservation scores, C50, C70, and C90, corresponding to the fraction of contacts maintained in at least 50, 70, and 90% of the analyzed frames, respectively (see Table 2), indicate that the interbarrel contacts are very well conserved during the MD simulations. The interbarrel residue−residue consensus contact map from the MD simulations of the WT, reported in Figure 7B, shows a strong similarity with the map of the X-ray structure of Figure 7A. Further, the paucity of gray spots in the map of Figure 7B also indicates a rigidity of the contacts at the interface. Indeed, a fraction close to 95% of them is conserved in at least 50% of the frames (C50 > 0.95), while 75% of them are conserved in at least 90% of the frames (C90 ∼ 0.75). Minor differences are observed between the WT and the mutants, indicating that the mutations, although they have an impact on the overall flexibility of the protein, as indicated by the PCA, have a negligible impact on the core interactions between the two barrels.

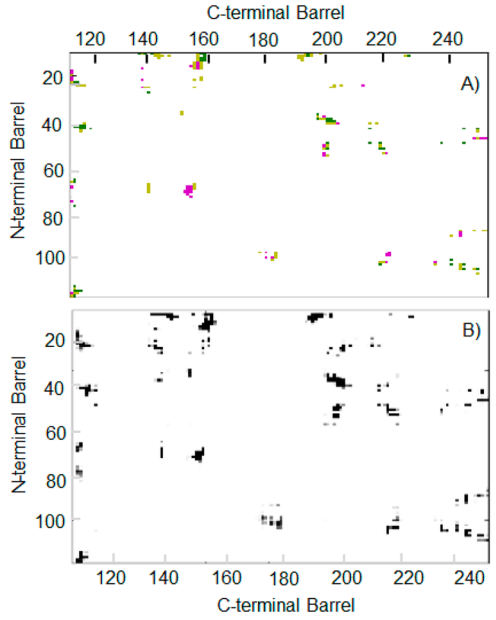

Figure 7. (A) Interbarrel residue−residue contact map of the X-ray structure plotted by COCOMAPS. Magenta, yellow, and green pixels in the map indicate hydrophilic−hydrophilic, hydrophilic−hydrophobic, and hydrophobic−hydrophobic contacts, respectively. (B) Interbarrel residue−residue consensus contact map from the MD simulations of the WT. The observed contacts are colored in gray scale to indicate their frequency during the MD simulation.

Table 2. Conservation Scores of the Interbarrel Residue−Residue Contacts

	C50	C70	C90
WT	0.955	0.856	0.753
D102N	0.949	0.847	0.745
G197D	0.964	0.852	0.764
T135M	0.977	0.863	0.745
V160A	0.958	0.883	0.756
G184S	0.950	0.843	0.743

Dynamics of Subpockets S1 and S4. The most important subpockets in the substrate recognition by FXa are S1 and S4.[9−12] As mentioned above, S1 is implicated in a strong salt bridge interaction between the conserved Asp189 located at its bottom and substrate Arg residues (prothrombin residues

dx.doi.org/10.1021/bi500770p | Biochemistry 2014, 53, 6992−7001

320 and 271), whereas S4 enhances the affinity for the substrate via van der Waals interactions. Therefore, we monitored the dynamics of these two subpockets by calculating their volume during the whole MD simulations, for all the considered systems (see Figure 8).

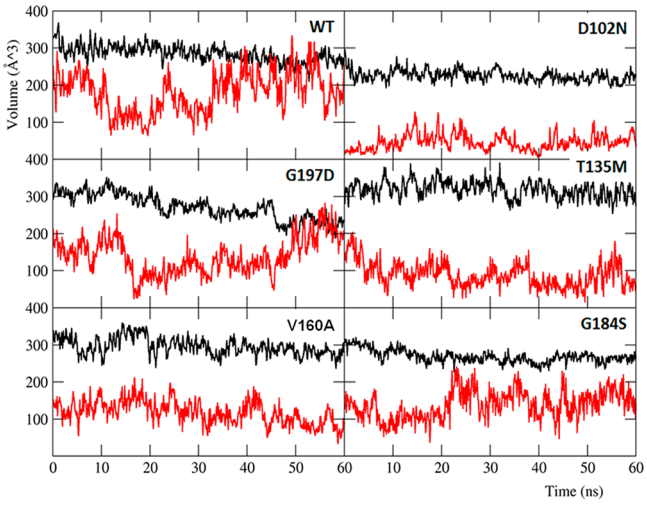

Figure 8. Time evolution of the volume of subpockets S1 and S4 along the MD simulations. Each point is the average volume from the four MD trajectories on a 100 ps window.

The definition of the pockets was performed independently for each system using the whole trajectory, which explains the rather different starting values. This choice was mandatory because of the changes in the shape of the much more flexible subpocket S4 in the different systems (see below), which did not allow a common pocket definition. On the other hand, subpocket S1 was found to be much more stable during the dynamics, regardless of which system was considered. With this caveat in mind, inspection of Figure 8 clearly indicates that subpocket S1 has approximately similar volumes in all the systems, which is also confirmed by the rather similar average volumes in Table 3.

Table 3. Average Volumes (cubic angstroms) and Relative Standard Deviations of Subpockets S1 and S4, from Cumulative Analysis of the Four MD Trajectories for Each System

	S1		S4	
	average	standard deviation	average	standard deviation
WT	285	22	179	54
D102N	226	15	46	21
G197D	271	35	139	49
T135M	318	23	88	33
V160A	296	24	118	32
G184S	268	17	138	38

The average volume of subpocket S1 during the dynamics of the WT, 285 Å^3, is also extremely close to the value of 277 Å^3 in the X-ray structure, confirming again the stability of this subpocket. With regard to the mutants, the only meaningful differences from the WT are in T135M, with a somewhat larger S1 subpocket, and D102N, with a clearly smaller S1 subpocket. The standard deviation for the S1 volume during the MD, on average <10%, is also indicative of a rather stable pocket.

Quite different is instead the behavior of subpocket S4, which highly fluctuates in the WT, with a standard deviation amounting to 30% of the total volume. Further, the average volume of this pocket from the MD simulations, 179 Å^3, is clearly smaller than the value of 259 Å^3 in the X-ray structure, indicating again that subpocket S4 is rather more flexible. Rather similar behavior was observed for all the mutants. As for the average volumes, the data reported in Table 3 indicate that the volume of subpocket S4 strongly depends on the specific mutant considered, with the largest deviation from the WT calculated again for T135M and D102N. In both cases, subpocket S4 was found to be clearly smaller than in the WT.

To gain a better understanding of the structural changes causing the large variation in the volume of subpocket S4, we compared the X-ray structure with selected frames from the MD simulations (see Figure 9). As shown in Figure 9,

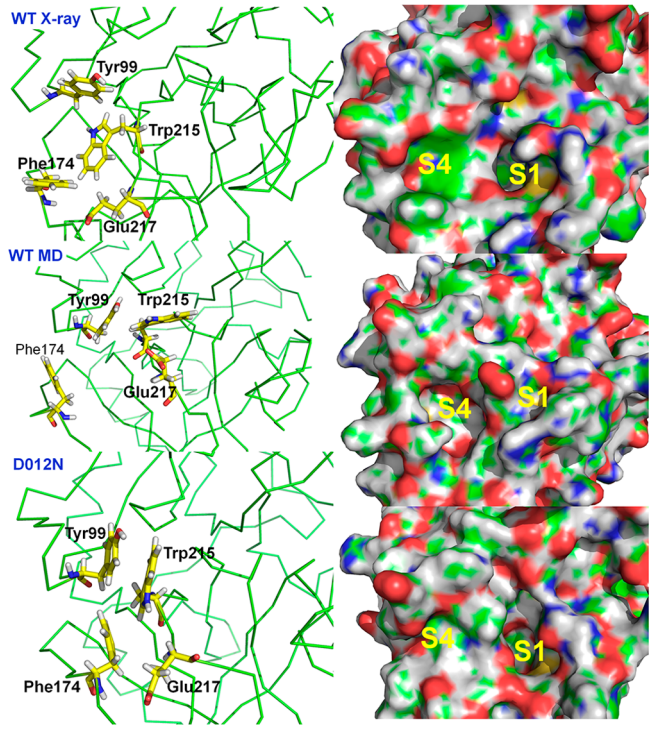

Figure 9. Ribbon and van der Waals representation of the region around subpockets S1 and S4 in the X-ray structure of the WT, in a selected frame of the MD simulation of the WT, and in a selected frame of the MD simulation of mutant D102N.

subpocket S4 is rather broad in the X-ray structure, with the side chain of Trp215 representing the floor of the pocket, and the side chains of Tyr99 and Phe174 representing the walls of this substantially hydrophobic and aromatic subpocket.

However, as evidenced by the PCA, during the dynamics we consistently observed rearrangement of these three residues, with a tendency of Trp215 to jump from the bottom of the pocket to the border of the S1 subpocket. This is due to the switch of Trp215 ϕ from −150° to roughly −65°, as shown in Figure 6, and to the concerted switch of the χ_1 angle (see Figure S11 of the Supporting Information) determining the orientation of the side chain of Trp215 from 60° to roughly −160°, closing the S1 subpocket entrance (see Figure 9). After this movement, Trp215 can engage in a stabilizing $\pi-\pi$ stacking interaction with the side chain of Tyr99 (Figure 9). Similar structural changes were observed in basically all the

dx.doi.org/10.1021/bi500770p | *Biochemistry* 2014, 53, 6992−7001

mutants. In all the cases, the aromatic side chains of Tyr99, Phe174, and Trp215 were engaged in some sort of stabilizing $\pi-\pi$ stacking interaction. Nevertheless, it is worth remarking that a similar $\pi-\pi$ stacking interaction is also established in T135M, without the rearrangement of Trp215 ϕ, with almost complete closure of the S4 subpocket, as evidenced in Figure 8. The time evolution of the distance between the baricenter of the side chain of Trp215 and that of Tyr99 and Phe174 (see Figure S12 of the Supporting Information) indicates that the conformational changes mentioned above have a minimal impact on the distance between the side chains of Trp215 and Tyr99, which stays quite stable around 5.0 Å. On the other hand, the distance between the side chains of Trp215 and Phe174 is quite more dynamic in the WT, G197D, and G184S, with fluctuations in the range of 5−15 Å. This is consistent with the clearly larger average S4 volume for the systems mentioned above (see Table 3). The Trp215−Phe174 distance is instead substantially flat around 5 Å for T135M and has minimal fluctuations for D102N, which is consistent with their smaller S4 average volume (see Table 3).

Mutant D102N, whose dynamics results in a rather small and stable S4 subpocket, deserves one mention. In this case, the side chains of Tyr99, Phe174, and Trp215 are able to engage in a $\pi-\pi$ stacked aggregate, very stable over time, that closes subpocket S4 almost completely. Finally, our results are consistent with previous MD studies, indicating a highly dynamic behavior of S4 residues in the WT FXa system.[66,67]

DISCUSSION AND CONCLUSIONS

A functional FXa enzyme is crucial for maintaining correct hemostasis. Remarkably, it has also been shown that a properly modified FXa enzyme may provide an effective strategy for the treatment of bleeding conditions.[18] The numerous forms of defective FXa isolated in patients suffering from bleeding symptoms thus represent an unmined gold reserve, both for understanding in detail the function of FXa and possibly for providing the basis for the design of novel modified enzymes for the treatment of hemostasis defects.

Herein, we present a molecular dynamics study of a pool of five natural FXa single-point mutants, selected to have only their catalytic efficiency affected by the mutation. Four independent simulations were obtained and analyzed for each system. The rmsd and rmsf values from the starting structure evidence no clear effect of the point mutations on enzyme stability, either globally or locally. Analysis by MDcons[47] shows that the interaction between the N- and C-terminal barrels is also well conserved in all the analyzed systems. This is not surprising, considering that the investigated mutants show a residual catalytic activity that would be incompatible with a completely misfolded protein.

Nevertheless, our comparative analysis of the dynamics of the systems still highlights differences between the mutants and the WT. The total number of hydrogen bonds is increased on average by 2−4 in three of the five mutants, G197D, G184S, and V160A, suggesting a stiffening of the systems upon mutation (whereas in T102N and T135M, it is slightly reduced, because of the loss of one hydrogen bond directly involving the mutated residue, with residues His57 and Glu159, respectively). More importantly, the PCA we performed on a combined trajectory of the four independent simulations, for a total of 200 ns for each system, clearly allowed us to highlight significant differences in the conformational space sampled by the WT FXa and the five mutants. WT FXa PC1 consists of a wide breathing movement between the N- and C-terminal barrels, mainly involving four loops around subpockets S1 and S4. This is in line with previous results reporting that the flexibility of enzyme binding sites is usually confined to solvent-exposed loops and turns, while residues directly involved in catalysis are usually less affected.[68]

When the trajectory is projected on the plane defined by the first two essential modes, it clearly appears that the WT and all the mutants explore two different minima. The only exception is T135M, which is trapped in one single minimum. Characterization of structures corresponding to the different minima in the various systems allowed us to localize the conformational changes around residues Phe174 and Trp215, which participate to shape the aromatic S4 subpocket. While the WT and all the mutants can oscillate between the two conformational minima, with the WT and G197D behaving quite similarly, T135 is trapped in the minimum corresponding to the X-ray conformation. Analysis of the traces of the covariance matrix indicated that the WT and G197D have similar overall flexibility, while the overall amount of motion spanned by the remaining mutants is reduced, with V160A and G184S being less flexible. The highest rigidity of V160A and G184S from the PCA also nicely matches the higher number of H-bonds in these two mutants.

Analysis of subpockets S1 and S4 highlighted the fact that the size of the S1 subpocket is generally unaffected by the mutations, although in T135M it is clearly larger than in the WT. On the other hand, the size of the S4 subpocket, which is consistent with the PCA, is clearly affected by the mutations. Again, G197D behaves quite like the WT, in terms of subpocket size and flexibility, while the other mutants have either clearly smaller or rigid subpockets.

Overall, our analysis suggests that four of the five considered mutants, D102N, T135M, V160A, and G184S, have rigidity clearly higher than that of the WT, in terms of both overall protein motion and subpocket S4 flexibility, which may impact substrate recognition. The other examined mutant, G197D, from a dynamic point of view is instead quite similar to the WT. Considering that the mutated Gly197 is placed in the proximity of the catalytic triad, its substitution with a negatively charged Asp could impact the catalytic step, rather than protein flexibility.

In conclusion, the finding that several mutations of FXa increase the overall protein rigidity agrees with the stiffening of FXa, caused by another recurrent substitution, we recently reported[21] and, more generally, with the current view of enzymes as molecules that have evolved under synergistic pressure between structure and dynamics, with their motions underlying catalysis.[69] Therefore, our results, showing that the pathogenic mutations compromise the FXa flexibility, provide a consistent explanation for the loss of catalytic efficiency of the analyzed FXa mutants.

ASSOCIATED CONTENT

Supporting Information

Movies of the first two PCs for all the systems and additional analyses. This material is available free of charge via the Internet at http://pubs.acs.org.

AUTHOR INFORMATION

Corresponding Author

*E-mail: luigi.cavallo@kaust.edu.sa.

Funding

Research reported in this publication was supported by the King Abdullah University of Science and Technology.

Notes

The authors declare no competing financial interest.

■ ACKNOWLEDGMENTS

This research was supported by the King Abdullah University of Science and Technology. We thank the KAUST Supercomputer Laboratory for generous access to computational resources.

■ REFERENCES

(1) Furie, B., and Furie, B. C. (1988) The molecular basis of blood coagulation. *Cell 53*, 505−518.

(2) Padmanabhan, K., Padmanabhan, K. P., Tulinsky, A., Park, C. H., Bode, W., Huber, R., Blankenship, D. T., Cardin, A. D., and Kisiel, W. (1993) Structure of Human Des(1−45) Factor-Xa at 2.2-Angstrom Resolution. *J. Mol. Biol. 232*, 947−966.

(3) Herrmann, F. H., Auerswald, G., Ruiz-Saez, A., Navarrete, M., Pollmann, H., Lopaciuk, S., Batorova, A., and Wulff, K. (2006) Factor X deficiency: Clinical manifestation of 102 subjects from Europe and Latin America with mutations in the factor 10 gene. *Haemophilia 12*, 479−489.

(4) Davie, E. W., Fujikawa, K., and Kisiel, W. (1991) The Coagulation Cascade: Initiation, Maintenance, and Regulation. *Biochemistry 30*, 10363−10370.

(5) Riddel, J. P., Aouizerat, B. E., Miaskowski, C., and Lillicrap, D. P. (2007) Theories of blood coagulation. *Journal of Pediatric Oncology Nursing 24*, 123−131.

(6) Hopfner, K. P., Lang, A., Karcher, A., Sichler, K., Kopetzki, E., Brandstetter, H., Huber, R., Bode, W., and Engh, R. A. (1999) Coagulation factor IXa: The relaxed conformation of Tyr99 blocks substrate binding. *Structure 7*, 989−996.

(7) Nagata, T., Yoshino, T., Haginoya, N., Yoshikawa, K., Isobe, Y., Furugohri, T., and Kanno, H. (2007) Cycloalkanediamine derivatives as novel blood coagulation factor Xa inhibitors. *Bioorg. Med. Chem. Lett. 17*, 4683−4688.

(8) Zbinden, K. G., Anselm, L., Banner, D. W., Benz, J., Blasco, F., Decoret, G., Himber, J., Kuhn, B., Panday, N., Ricklin, F., Risch, P., Schlatter, D., Stahl, M., Thomi, S., Unger, R., and Haap, W. (2009) Design of novel aminopyrrolidine factor Xa inhibitors from a screening hit. *Eur. J. Med. Chem. 44*, 2787−2795.

(9) Hedstrom, L. (2002) Serine protease mechanism and specificity. *Chem. Rev. 102*, 4501−4523.

(10) Nazare, M., Will, D. W., Matter, H., Schreuder, H., Ritter, K., Urmann, M., Essrich, M., Bauer, A., Wagner, M., Czech, J., Lorenz, M., Laux, V., and Wehner, V. (2005) Probing the subpockets of factor Xa reveals two binding modes for inhibitors based on a 2-carboxyindole scaffold: A study combining structure-activity relationship and X-ray crystallography. *J. Med. Chem. 48*, 4511−4525.

(11) Salonen, L. M., Holland, M. C., Kaib, P. S. J., Haap, W., Benz, J., Mary, J. L., Kuster, O., Schweizer, W. B., Banner, D. W., and Diederich, F. (2012) Molecular Recognition at the Active Site of Factor Xa: Cation-π Interactions, Stacking on Planar Peptide Surfaces, and Replacement of Structural Water. *Chem.—Eur. J. 18*, 213−222.

(12) Rai, R., Sprengeler, P. A., Elrod, K. C., and Young, W. B. (2001) Perspectives on factor Xa inhibition. *Curr. Med. Chem. 8*, 101−119.

(13) Bhunia, S. S., Roy, K. K., and Saxena, A. K. (2011) Profiling the Structural Determinants for the Selectivity of Representative Factor-Xa and Thrombin Inhibitors Using Combined Ligand-Based and Structure-Based Approaches. *J. Chem. Inf. Model. 51*, 1966−1985.

(14) Katsnelson, M., Sacco, R. L., and Moscucci, M. (2012) Progress for Stroke Prevention with Atrial Fibrillation Emergence of Alternative Oral Anticoagulants. *Circulation 125*, 1577−1583.

(15) Agnelli, G., Buller, H. R., Cohen, A., Curto, M., Gallus, A. S., Johnson, M., Masiukiewicz, U., Pak, R., Thompson, J., Raskob, G. E., Weitz, J. I., and Investigators, A. (2013) Oral Apixaban for the Treatment of Acute Venous Thromboembolism. *N. Engl. J. Med. 369*, 799−808.

(16) Agnelli, G., Buller, H. R., Cohen, A., Curto, M., Gallus, A. S., Johnson, M., Porcari, A., Raskob, G. E., Weitz, J. I., and Investigators, A.-E. (2013) Apixaban for Extended Treatment of Venous Thromboembolism. *N. Engl. J. Med. 368*, 699−708.

(17) Menegatti, M., and Peyvandi, F. (2009) Factor X Deficiency. *Semin. Thromb. Hemostasis 35*, 407−415.

(18) Ivanciu, L., Toso, R., Margaritis, P., Pavani, G., Kim, H., Schlachterman, A., Liu, J. H., Clerin, V., Pittman, D. D., Rose-Miranda, R., Shields, K. M., Erbe, D. V., Tobin, J. F., Arruda, V. R., and Camire, R. M. (2011) A zymogen-like factor Xa variant corrects the coagulation defect in hemophilia. *Nat. Biotechnol. 29*, 1028−1033.

(19) Li, H. J., Haurigot, V., Doyon, Y., Li, T. J., Wong, S. N. Y., Bhagwat, A. S., Malani, N., Anguela, X. M., Sharma, R., Ivanciu, L., Murphy, S. L., Finn, J. D., Khazi, F. R., Zhou, S. Z., Paschon, D. E., Rebar, E. J., Bushman, F. D., Gregory, P. D., Holmes, M. C., and High, K. A. (2011) In vivo genome editing restores haemostasis in a mouse model of haemophilia. *Nature 475*, 217−221.

(20) http://www.isth.org/?MutationsRareBleedin.

(21) Menegatti, M., Vangone, A., Palla, R., Milano, G., Cavallo, L., Oliva, R., De Cristofaro, R., and Peyvandi, F. (2014) A recurrent Gly43Asp substitution in coagulation Factor X rigidifies its catalytic pocket and impairs catalytic activity and intracellular trafficking. *Thromb. Res. 133*, 481−487.

(22) Rudolph, A. E., Porche-Sorbet, R., and Miletich, J. P. (2000) Substitution of asparagine for arginine 347 of recombinant factor Xa markedly reduces factor Va binding. *Biochemistry 39*, 2861−2867.

(23) Pinotti, M., Monti, M., Boroni, M., Marchetti, G., and Bernardi, F. (2004) Molecular characterization of factor X deficiency associated with borderline plasma factor X levels. *Haematologica 89*, 501−502.

(24) Isshiki, I., Favier, R., Moriki, T., Uchida, T., Ishihara, H., Van Dreden, P., Murata, M., and Ikeda, Y. (2005) Genetic analysis of hereditary factor X deficiency in a French patient of Sri Lankan ancestry: In vitro expression study indentified Gly366Ser substitution as the molecular basis of the dysfunctional factor X. *Blood Coagulation Fibrinolysis 16*, 9−16.

(25) Pinotti, M., Camire, R. M., Baroni, M., Rajab, A., Marchetti, G., and Bernardi, F. (2003) Impaired prothrombinase activity of factor X Gly381 Asp results in severe familial CRM+ FX deficiency. *Thromb. Haemostasis 89*, 243−248.

(26) Messier, T. L., Wong, C. Y., Bovill, E. G., Long, G. L., and Church, W. R. (1996) Factor X Stockton: A mild bleeding diathesis associated with an active site mutation in factor X. *Blood Coagulation Fibrinolysis 7*, 5−14.

(27) Millar, D. S., Elliston, L., Deex, P., Krawczak, M., Wacey, A. I., Reynaud, J., Nieuwenhuis, H. K., Bolton-Maggs, P., Mannucci, P. M., Reverter, J. C., Cachia, P., Pasi, K. J., Layton, D. M., and Cooper, D. N. (2000) Molecular analysis of the genotype-phenotype relationship in factor X deficiency. *Hum. Genet. 106*, 249−257.

(28) Odom, M. W., Leone, G., Destefano, V., Montiel, M. M., Boland, E. J., Anderson, J., and Jagadeeswaran, P. (1994) 5 Novel Point Mutations: 2 Causing Hemophilia-B and 3 Causing Factor-X Deficiency. *Mol. Cell. Probes 8*, 63−65.

(29) Hess, B., Kutzner, C., van der Spoel, D., and Lindahl, E. (2008) GROMACS 4: Algorithms for highly efficient, load-balanced, and scalable molecular simulation. *J. Chem. Theory Comput. 4*, 435−447.

(30) Wallnoefer, H. G., Handschuh, S., Liedl, K. R., and Fox, T. (2010) Stabilizing of a Globular Protein by a Highly Complex Water Network: A Molecular Dynamics Simulation Study on Factor Xa. *J. Phys. Chem. B 114*, 7405−7412.

(31) Sali, A., and Blundell, T. L. (1993) Comparative Protein Modeling by Satisfaction of Spatial Restraints. *J. Mol. Biol. 234*, 779−815.

(32) Hornak, V., Abel, R., Okur, A., Strockbine, B., Roitberg, A., and Simmerling, C. (2006) Comparison of multiple amber force fields and development of improved protein backbone parameters. *Proteins 65*, 712−725.

(33) Jorgensen, W. L., Duffy, E. M., and Tiradorives, J. (1993) Computational investigations of protein denaturation: Apomyoglobin and Chaotrope-Arene interactions. *Philos. Trans. R. Soc., A 345*, 87−96.
(34) Darden, T., York, D., and Pedersen, L. (1993) Particle Mesh Ewald: An N.Log(N) Method for Ewald Sums in Large Systems. *J. Chem. Phys. 98*, 10089−10092.
(35) Lemak, A. S., and Balabaev, N. K. (1994) On the Berendsen Thermostat. *Mol. Simul. 13*, 177−187.
(36) Martonak, R., Laio, A., and Parrinello, M. (2003) Predicting crystal structures: The Parrinello-Rahman method revisited. *Phys. Rev. Lett. 90*, 1−4.
(37) Durrant, J. D., and McCammon, J. A. (2011) HBonanza: A computer algorithm for molecular-dynamics-trajectory hydrogen-bond analysis. *J. Mol. Graphics Modell. 31*, 5−9.
(38) Skjaerven, L., Martinez, A., and Reuter, N. (2011) Principal component and normal mode analysis of proteins; a quantitative comparison using the GroEL subunit. *Proteins 79*, 232−243.
(39) Levy, R. M., Srinivasan, A. R., Olson, W. K., and Mccammon, J. A. (1984) Quasi-Harmonic Method for Studying Very Low-Frequency Modes in Proteins. *Biopolymers 23*, 1099−1112.
(40) Ichiye, T., and Karplus, M. (1991) Collective Motions in Proteins: A Covariance Analysis of Atomic Fluctuations in Molecular-Dynamics and Normal Mode Simulations. *Proteins: Struct., Funct., Genet. 11*, 205−217.
(41) Amadei, A., Linssen, A. B. M., and Berendsen, H. J. C. (1993) Essential dynamics of proteins. *Proteins: Struct., Funct., Genet. 17*, 412−425.
(42) Bakan, A., Meireles, L. M., and Bahar, I. (2011) ProDy: Protein Dynamics Inferred from Theory and Experiments. *Bioinformatics 27*, 1575−1577.
(43) Humphrey, W., Dalke, A., and Schulten, K. (1996) VMD: Visual molecular dynamics. *J. Mol. Graphics Modell. 14*, 33−38.
(44) Schmidtke, P., Bidon-Chanal, A., Luque, F. J., and Barril, X. (2011) MDpocket: Open-source cavity detection and characterization on molecular dynamics trajectories. *Bioinformatics 27*, 3276−3285.
(45) Schmidtke, P., Le Guilloux, V., Maupetit, J., and Tuffery, P. (2010) fpocket: Online tools for protein ensemble pocket detection and tracking. *Nucleic Acids Res. 38*, W582−W589.
(46) (a) Vangone, A., Oliva, R., and Cavallo, L. (2012) CONS-COCOMAPS: A novel tool to measure and visualize the conservation of inter-residue contacts in multiple docking solutions. *BMC Bioinf. 13*, 1−9. (b) Vangone, A., Spinelli, R., Scarano, V., Cavallo, L., and Oliva, R. (2011) COCOMAPS: a web application to analyze and visualize contacts at the interface of biomolecular complexes. *Bioinformatics 27*, 2915−2916.
(47) Abdel-Azeim, S., Chermak, E., Vangone, A., Oliva, R., and Cavallo, L. (2014) MDcons: Intermolecular contact maps as a tool to analyze the interface of protein complexes from molecular dynamics trajectories. *BMC Bioinf. 15*, 1−11.
(48) Lensink, M. F., Mendez, R., and Wodak, S. J. (2007) Docking and scoring protein complexes: CAPRI 3rd edition. *Proteins 69*, 704−718.
(49) Oliva, R., Vangone, A., and Cavallo, L. (2013) Ranking multiple docking solutions based on the conservation of inter-residue contacts. *Proteins 81*, 1571−1584.
(50) Vangone, A., Cavallo, L., and Oliva, R. (2013) Using a consensus approach based on the conservation of inter-residue contacts to rank CAPRI models. *Proteins 81*, 2210−2220.
(51) Maisuradze, G. G., Liwo, A., and Scheraga, H. A. (2009) Principal Component Analysis for Protein Folding Dynamics. *J. Mol. Biol. 385*, 312−329.
(52) Novikov, G. V., Sivozhelezov, V. S., and Shaitan, K. V. (2013) Functionally relevant conformational dynamics of water-soluble proteins. *Mol. Biol. 47*, 149−160.
(53) Skjaerven, L., Muga, A., Reuter, N., and Martinez, A. (2012) A dynamic model of long-range conformational adaptations triggered by nucleotide binding in GroEL-GroES. *Proteins 80*, 2333−2346.
(54) Papaleo, E., Mereghetti, P., Fantucci, P., Grandori, R., and De Gioia, L. (2009) Free-energy landscape, principal component analysis, and structural clustering to identify representative conformations from molecular dynamics simulations: The myoglobin case. *J. Mol. Graphics Modell. 27*, 889−899.
(55) Altis, A., Otten, M., Nguyen, P. H., Hegger, R., and Stock, G. (2008) Construction of the free energy landscape of biomolecules via dihedral angle principal component analysis. *J. Chem. Phys. 128*, 245102.
(56) Li, L., and Szostak, J. W. (2014) The Free Energy Landscape of Pseudorotation in 3′-5′ and 2′-5′ Linked Nucleic Acids. *J. Am. Chem. Soc. 136*, 2858−2865.
(57) Sicard, F., and Senet, P. (2013) Reconstructing the free-energy landscape of Met-enkephalin using dihedral principal component analysis and well-tempered metadynamics. *J. Chem. Phys. 138*, 1−14.
(58) Maisuradze, G. G., Liwo, A., and Scheraga, H. A. (2010) Relation between Free Energy Landscapes of Proteins and Dynamics. *J. Chem. Theory Comput. 6*, 583−595.
(59) Hu, J. P., Liu, M., Tang, D. Y., and Chang, S. (2013) Substrate Recognition and Motion Mode Analyses of PFV Integrase in Complex with Viral DNA via Coarse-Grained Models. *PLoS One 8*, e54929.
(60) Amadei, A., Ceruso, M. A., and Di Nola, A. (1999) On the convergence of the conformational coordinates basis set obtained by the essential dynamics analysis of proteins' molecular dynamics simulations. *Proteins: Struct., Funct., Genet. 36*, 419−424.
(61) Lou, H. F., and Cukier, R. I. (2006) Molecular dynamics of apo-adenylate kinase: A principal component analysis. *J. Phys. Chem. B 110*, 12796−12808.
(62) Yang, L., Song, G., Carriquiry, A., and Jernigan, R. L. (2008) Close correspondence between the motions from principal component analysis of multiple HIV-1 protease structures and elastic network modes. *Structure 16*, 321−330.
(63) Batista, P. R., Robert, C. H., Marechal, J. D., Ben Hamida-Rebai, M., Pascutti, P. G., Bisch, P. M., and Perahia, D. (2010) Consensus modes, a robust description of protein collective motions from multiple-minima normal mode analysis-application to the HIV-1 protease. *Phys. Chem. Chem. Phys. 12*, 2850−2859.
(64) Tama, F., and Sanejouand, Y. H. (2001) Conformational change of proteins arising from normal mode calculations. *Protein Eng. 14*, 1−6.
(65) Levigne, S., Thiec, F., Cherel, G., Irving, J. A., Fribourg, C., and Christophe, O. D. (2007) Role of the α-helix 163−170 in factor Xa catalytic activity. *J. Biol. Chem. 282*, 31569−31579.
(66) Singh, N., and Briggs, J. M. (2008) Molecular Dynamics Simulations of Factor Xa: Insight into Conformational Transition of Its Binding Subsites. *Biopolymers 89*, 1104−1113.
(67) Wang, J. F., Hao, P., Li, Y. X., Dai, J. L., and Li, X. (2012) Exploration of conformational transition in the aryl-binding site of human FXa using molecular dynamics simulations. *J. Mol. Model. 18*, 2717−2725.
(68) Luque, I., and Freire, E. (2000) Structural stability of binding sites: Consequences for binding affinity and allosteric effects. *Proteins: Struct., Funct., Genet.* No. Suppl. 4, 63−71.
(69) Eisenmesser, E. Z., Millet, O., Labeikovsky, W., Korzhnev, D. M., Wolf-Watz, M., Bosco, D. A., Skalicky, J. J., Kay, L. E., and Kern, D. (2005) Intrinsic dynamics of an enzyme underlies catalysis. *Nature 438*, 117−121.